A very wide field focusing telescope for synoptic studies in the soft X-ray band

Paul Gorenstein
Harvard-Smithsonian Center for Astrophysics
Cambridge, MA 02138 USA

Abstract

Constructing synoptic telescopes is a current trend in astronomy. Pan-STARRS and the Large Synoptic Survey Telescope (LSST) are examples in the optical band. It is the motivation of many scientists who advocate on behalf of the Square Kilometer Array radio telescope. The coded mask detectors of **Swift** and the future, more powerful **EXIST,** cover the hard X-ray band. The soft X-ray band perhaps hosts the largest range of variable sources. It includes stars, compact binaries, supernova, SMBH's, as well as the X-ray components of Gamma-Ray Bursts and their soft X-ray afterglows. Unlike the hard X-ray band coverage of the soft X-ray band can utilize focusing telescopes and we describe a very wide field focusing instrument with an angular resolution of a few arc minutes that can view every position in the sky for 2×10^4 seconds every 24 hours. While gathering considerable information on its own it finds new targets or ones that are experiencing a change in state for very high throughput pointed telescopes and very high resolution spectrometers to study in-depth. The concept is not new but has become more relevant recently with the discovery of more variable phenomena and more feasible with the impending development of position sensitive CMOS detector arrays that can cover areas exceeding a square meter and the availability of relatively inexpensive, light weight substrate materials. An instrument with significant collecting area would be compatible with a NASA Small Explorer mission.

1. Introduction

1.1 Variability

Temporal variability is the most remarkable feature of the X-ray sky. Among the compact binaries within our galaxy, times scales range from millisecond pulsars to transient source outbursts at decadal intervals. Observing changes in their intensities and spectra are among the few means of studying black holes, neutron stars and testing general relativity. There is a background of random occurring X-ray flares from young and pre-main sequence stellar clusters indicating the presence of star formation. The extragalactic sky contains the most rapidly varying sources, gamma-ray bursts and X-ray flashes that exist for intervals ranging from milliseconds to minutes. The most recent new discovery of rapid intensity variations in the extragalactic sky is a 400 second long soft X-ray flare from a supernova explosion detected serendipitously in the field of the ***Swift* XRT** (Soderberg et al, 2008). At the other extreme, changes in the intensity of an AGN can occur over a time span up to years, reflecting changes in jet activity or possibly triggered by the central SMBH tidally disrupting and accreting a star (Halpern et al, 2008, Esquej et al, 2008, or being obscured by an orbiting cloud (Risaliti et, 2010, Wang et al, 2010).

The importance of observing temporal variations in the X-ray band and advocating developing the next generation of instrumentation to do so are subjects of White Papers submitted to the NAS Astronomy Decadel Survey Committee. In their paper entitled "Scientific Productivity with X-ray All-Sky Monitors" Remillard, Levine, and McClintock, 2009 evaluate the results of a decade and a half of operations of the ***Rossi X-ray Timing Explorer*** and offer compelling reasons for developing a more advanced X-ray all-sky monitor than the **ASM** of ***RXTE***, and Japan's ***MAXI*** (installed on the Japanese Module of the International Space Station). Addressing extra-galactic as well as galactic temporal variations, a large community of authors submitted a White Paper, entitled "The Dynamic X-ray Sky of the Local Universe" (Soderberg et al, 2009). Their key goals include detecting supernova at the time of explosion, observing stars with active coronas, detecting quiescent supermassive black holes and "exploring new phase space of the Transient Universe at X-ray wavelengths". They refer specifically to the ***EXIST*** mission concept (Grindlay 2005) as satisfying those objectives in the hard X-ray band. With the discovery of soft X-ray flares from supernova, the existence of "X-ray flashes" and "orphan afterglows" from gamma-ray bursts those goals also apply also to a soft X-ray wide field detector system that would be operating in parallel.

Detecting and obtaining precise positions for very short lived events from random locations requires an all-sky monitor with a very large field of view. Scanning detectors with a low instantaneous field of view like the ***RXTE* ASM** and ***MAXI*** are not the optimum type tool. They will miss many short duration events and obtain only intermittent samples of those that are longer lived. Wide field **c**oded mask detectors, for example the ***Swift* BAT** and ***EXIST*** do fulfill this requirement and in fact are the only option for the hard X-ray/soft gamma-ray regime. In the soft X-ray band a similar type of coded mask instrument would encounter a much larger background rate from diffuse cosmic X-rays, and the intense discrete X-rays sources. It is also more likely to encounter variability from several directions occurring simultaneously. A focusing telescope is a more appropriate tool for this environment.

We describe a concept for a focusing very wide field soft X-ray telescope with a large dynamic range that is capable of resolving individual transients in a field with multiple variable objects. It

has a field of view of nearly 4 steradians. By following a pointing program similar to **BAT's** (***Swift***) or **LAT's** (***Fermi***) nearly every point in the sky that is visible from low Earth orbit can be observed nearly continuously. The prime bandwidth for detecting transients and measuring positions with sub-arc minute precision is 0.5 to 8 keV. However, the bandwidth continues to over 15 keV with less angular resolution and lower sensitivity. The higher energy band can be a source of useful information on spectra and timing. Based upon a preliminary conceptual design, by unfolding and expanding the telescope in orbit the system described in this paper will fit within the dynamic envelope of spacecraft compatible with NASA's Small Explorer missions.

1.2 Instrument Description

The instrument is a hybrid of a "lobster-eye" telescope that focuses in one dimension and a coded mask for angular resolution the other. It has less effective area than a two dimensional coded mask system of similar size, but has the advantage of much lower background from diffuse X-rays and being able to image all the discrete sources within the field of view, variable or steady onto distinct regions of the detector. Positions of transient events would be available very rapidly, essentially instantaneously in the focusing dimension and very quickly in the other by limiting the region that need be correlated with the coded mask to only a small fraction of the sky and only along one dimension. In comparison to a two-dimensional lobster-eye telescope of similar size (e.g. Fraser et al, 2002) the hybrid has more effective area, more bandwidth, and functions over a much larger dynamic range of intensity.

The concept is not new. The type of optics was described by Schmidt in 1975 and the hybrid focusing/coded mask concept was described by Gorenstein and Mauche in 1984. In both cases the description was not quantitative. Very small field of view telescopes were constructed (Gorenstein, et al, 1996, Hudec et al, 2003). However, the relevance of an all-sky X-ray monitor with a very broad field of view has become much more evident following the discovery of gamma-ray burst X-ray afterglows, X-ray flashes, the possibility of their being a less narrowly beamed X-ray component of gamma-ray bursts, the prospect of finding and identifying "orphan" X-ray afterglows that would augment the catalog by a considerable amount, and most recently the discovery of short lived X-ray flares from certain type supernova. Until very recently the absence of a very large format position sensitive X-ray detector system with good energy resolution had inhibited the development of very large field of view X-ray telescopes. Now there exists the capability to fabricate very large number of solid state position sensitive detectors with good energy resolution, such as CCDs, CMOS detectors, and silicon drift chambers (Janesick et al, 2009, Bongiorno et al, 2009). Also, very large area cylindrical gas electron multipliers (GEMS proportional counters) have been developed (Bencivenni, 2009).

The theoretical performance of a small instrument as determined by ray tracing is described in this paper.

2. Transient X-rays from Gamma-ray Bursts and Supernova

2.1 Gamma-rays Bursts, X-ray Flashes and X-ray Afterglows

It is well known that gamma-rays bursts are followed by an X-ray afterglow, which has been the key to optically identifying their host galaxy and measuring its redshift (Costa et al, 1997). In addition, there is a class of GRB-like events whose content is predominantly X-rays. ***BeppoSAX*** (Heise et al, 2001) and the ***HETE-2*** spacecraft (Sakamoto et al, 2005) detected bursts

that resemble GRBs in many respects but whose spectra were much softer and resided mostly in the 2 to 30 keV X-ray band. They named these events: "X-ray Flashes" (XRF). In addition ***HETE-2*** observed an intermediate class of events that they named "X-Ray Rich" (XRR) where the 2-30 keV fluence is comparable to the fluence above 30 keV. The ***Swift*** hard X-ray instrument **BAT** is not as sensitive as ***BeppoSAX*** and ***HETE-2*** to XRFs so aside from some coverage by the ***RXTE*** **ASM** not much more has been learned about them. It is generally agreed that GRBs are strongly beamed. This leaves open the possibility that the opening angle is energy dependent and that the softer photons or X-ray component of a GRB may have a larger opening angle. Woods and Loeb, 1999, suggested that X-ray flashes are GRBs but viewed at a larger angle off the center of the beam. Furthermore, one could expect that the X-ray afterglow which is most likely the product of a secondary shock wave or scattering would not be as strongly beamed. For this reason more sensitive all-sky exposures in the X-ray band may detect "orphan" X-ray afterglows (Rossi, Perna, and Daigne, 2008).

GRBs with very high redshift are the subject of much attention because of their connection to star formation in the early universe. In fact, the most distant object ever detected was the host galaxy of GRB 090423 with a redshift of 8.2 (Tanvir et al, 2009, Savaterra et al, 2009). The X-ray content of high z bursts is enhanced by the red shift. The behavior of the redshift as a function of the distance is such that at large values of z the redshift increases very rapidly as a function of distance or look-back time. Therefore, we can expect that for even slightly longer look back times than at z = 8 the intrinsic GRB spectrum would be softened considerably more. The sensitivity of searches for ever more distant gamma-ray bursts is likely to depend increasingly upon detecting their X-ray component.

2.2 Supernova

Fortuitously the onset of a supernova explosion was detected during an exposure of one of the ***Swift*** **XRT** GRB fields (Soderberg et al, 2008). A soft X-ray flare lasting about 400 seconds, occurred at a position quite distant from the X-ray afterglow of the GRB. Its peak flux of 6.9×10^{-10} ergs/cm^{-2} s^{-1} (0.3 to 10 keV) was relatively intense for a distant extragalaxtic X-ray source. Its spectrum was a power law with a photon index of 2.3 ± 0.3, and a hydrogen column density of 6.9×10^{21} cm^{-2}, in excess of the absorption within the Milky Way. Although the SN was within its field of view, **BAT,** the ***Swift*** hard X-ray detector, did not detect it.

Chevalier and Fransson, 2008 attribute the serendipitous discovery to the shock breakout emission from a normal Type Ib/c supernova. Soft X-ray flares are expected to occur also with some Type 2 supernova (Chevalier. Fransson, and Nymark, 2006). This view suggests that many soft X-ray flare events from supernova occur each year whose spectra are below the 15−150 keV band of the ***Swift*** **BAT**.

3. The Wide Field X-ray Telescope

3.1 Optics and Coded Mask

The telescope focuses in one dimension, i.e. to a line image and is a coded mask in the other. The optics are based upon the concept described by Schmidt, 1975. Angel, 1979, without knowledge of Schmidt's paper described how a two dimensional focusing telescope composed of square channels would function. Noting the similarity between the optics and the eyes of crustaceans Angel named it a "lobster-eye" telescope.

Due to reflection inefficiencies and structure that occludes part of the aperture a lobster-eye telescope has less collecting area than a coded mask with the same diameter and focal length. However, as focusing telescopes have demonstrated so convincingly the reduction in background that accrues from concentrating the X-rays from a specific direction onto a small area of the detector can overcome the collecting area deficit and be more sensitive.

The 1D lobster-eye geometry is shown in Fig. 1. Flat mirrors are evenly spaced around the circumference of a cylinder with their faces along a radius of the cylinder. Both faces of the reflectors are coated with Ir or Pt plus a thin C overcoat. They act either as a mirror or as a collimator depending upon whether the angle of incidence is more or less than the critical angle.

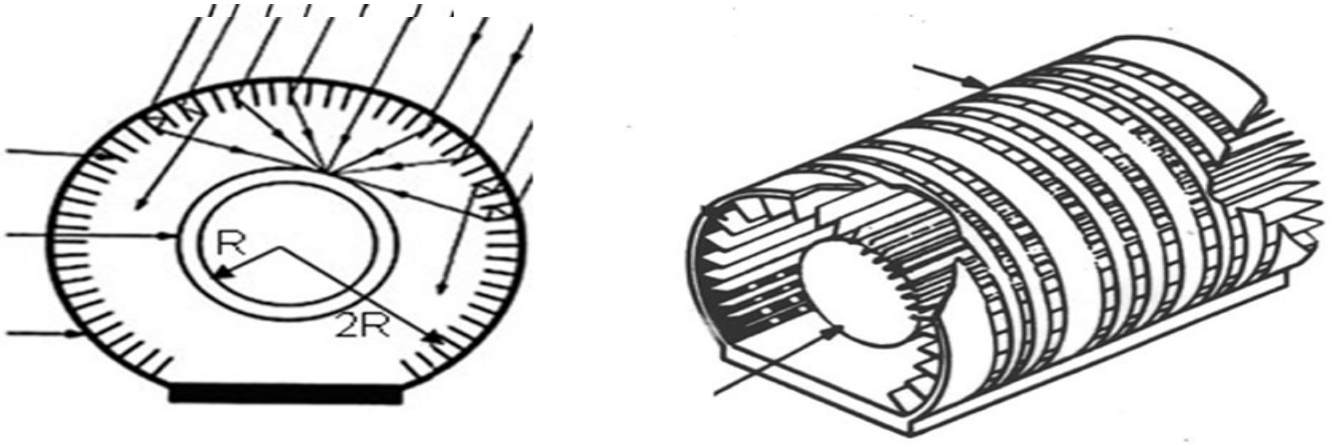

Fig. 1. The left panel shows X-rays from a fixed direction that are focused on to a cylindrical position sensitive detector whose radius is half that of the reflectors. Some rays arrive at the detector along their original direction but their angular range is limited by the collimation action of the reflectors. The right panel shows the coded mask, surrounding the reflectors. The mask contains a pseudo random distribution of open slits along the axis of a cylinder.

The point response of the optic for five energies as determined by ray tracing is shown in Fig. 2. It consists of a central peak plus a wider base of much lower amplitude. Note that the vertical scale is different for all of the energies. The central peak is composed of X-rays that are reflected an odd number of times, mostly just once but at low energies some that are reflected three times. The broad base consists of rays that miss the reflectors or are reflected an even number of times. At low energies a significant number survive two reflections after which they resume their original direction. Their extent is limited ultimately when the reflection angle exceeds the critical angle or by the collimating action of the reflectors. The relative power in these components varies as a function of energy. Below 3 keV the central peak accounts for 50% of the rays and the base under the peak for rest. The FWHM of the peak is about 3.5 arc minutes. As shown in Fig. 4 at higher energies a smaller fraction of the total flux is in the central peak.

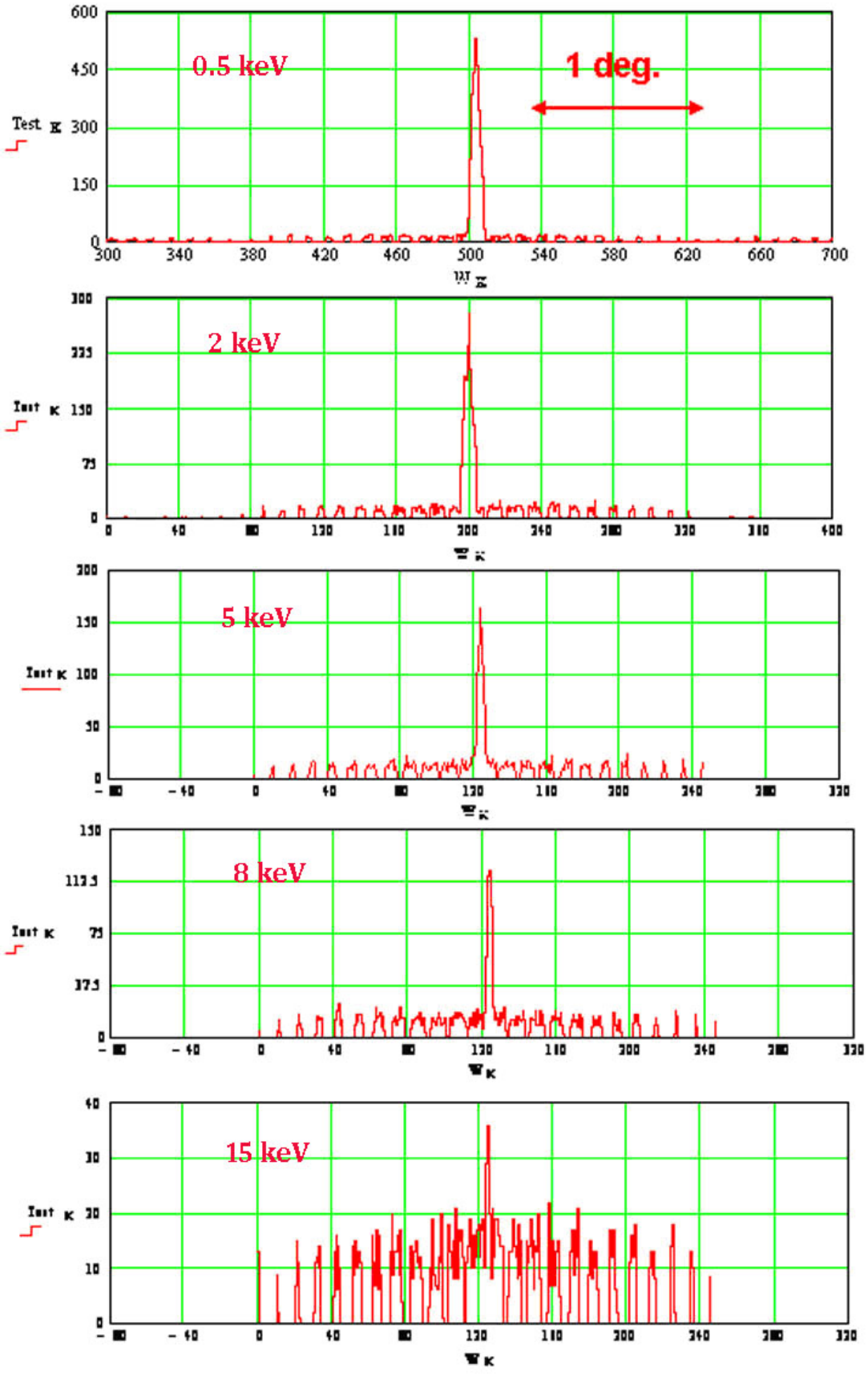
0.5 keV
1 deg.
2 keV
5 keV
8 keV
15 keV

Fig. 2. Point response of a lobster-eye telescope in one dimension for five energies as determined from ray tracing with statistical fluctuations. The horizontal scale is the same for all, 0.66 arc min per bin, but their origins differ. The vertical scale varies in order for the peaks be about the same height.. The top line of the scale of each are 600, 300, 200, 150, and 40 for 0.5 keV, 2 keV, 5 keV, 8 keV, and 15 keV respectively.

The coded mask that provides angular resolution in the other dimension consists of a pseudo random distribution of open semi-circle slits along the axis of the cylinder. It was not included in the ray tracing simulations but its transmission was assumed to be is 45% in estimating the effective area. It was also assumed that the open slits would not have a collimating effect that limits the range of polar angles with respect to the axis.

Comparison to a 2D lobster-eye telescope

The claim that a 1D focusing lobster-eye/coded mask hybrid telescope is preferable to a 2D coded mask for observing soft X-ray transients begs the question of whether a 2D focusing lobster-eye would be even better. In a 2D telescope the coded mask is replaced by an orthogonal set of reflectors that are either integrated with the first set or exist as a separate reflector array that is placed either behind or in front of the first, and the geometry is spherical instead of cylindrical. Its effective area, bandwidth, – and background are much smaller and its point response function is more complex with a smaller fraction of the flux in a point-like image and a larger fraction in the halo. After a sufficiently long exposure of a persistent source the 2D lobster-eye telescope would ultimately be more sensitive than the hybrid 1D telescope/coded mask. However, when the fluence of the burst or transient is low the 2D telescope could be photon limited or the position distorted by statistical fluctuations of the halo. If the GRB or XRF contains a very high instantaneous photon flux the 2D point source image could be affected by pile-up in the detector and submerged in the halo. The consequences are loss of accuracy in measuring positions, spectra, and timing. The long 1D line image of a point source will not be susceptible to pile-up.

Several on-going projects are devoted to the development of 2D lobster-eye telescopes for both space and industrial applications. A 2D telescope composed of square microchannel plates with a field of view of 162 x 22.5 degrees (~ 1 ster) and an effective area of about 4 cm^2 at 2 keV was developed by the Space Research Centre at the University of Leicester (Fraser et al, 2002) for the International Space Station. It has not yet been installed presumably because of ISS related issues. A great virtue of a microchannel plate telescope is very low mass. The theoretical angular resolution of the point component of the response function would be a few arcseconds if all channels were aligned perfectly along their intended directions. In practice the FWHM of the Leicester telescope point response function was 5 arcmin. The fraction of the flux that is within the FWHM was not stated. The development of square microchannel plate lobster-eye X-ray telescopes is continuing with both space and industrial applications as goals (Mutz et al, 2007).

Grubsky et al 2007 are developing 2D lobster-eye telescopes composed of interlocking silicon flats that form a square channel.

There is a new approach to X-ray optics based upon micro electromechanical systems (MEMS) (Mitsuishi et al, 2010) that may allow much lower mass telescopes than one based upon flat reflectors (although not lower mass than micro channel optics). Anisotropic wet etching of silicon produces open channels whose faces act as reflectors. The authors consider Wolter

telescopes but unlike the micro channel plate optics this approach is compatible with a 1D lobster-eye focusing telescope and if successful would have very good angular resolution. However, there are serious problems. It probably would not be possible to coat the silicon planes with a heavy metal that would result in a much larger critical angle and a broader bandwidth. Also if the figures that appear in Mitsuishi et al provide an accurate impression, the fraction of open area of the MEMS optics is low compared to the flat sheets of our design. Furthermore, the surface roughness of the channels that are etched is 6 nm, which is much poorer than the typical 0.5 nm roughness of glass reflectors.

4. Expected Performance

4.1 Telescope Parameters

The performance of the telescope was simulated with ray tracing. However its dimensions and other parameters were selected without the verification of feasibility that a true mechanical design would provide. Therefore, the simulated performance may be overly optimistic. For example, if the mirrors are made of glass, they may have to be thicker than the assumed value in order to remain flat and/or survive launch. Doubling their thickness would not have much effect upon the resolution or effective area of the telescope but would increase the mass.

All the reflectors are identical flats with each aligned along a radius of a cylinder and equally spaced around the circumference. They are spaced by 6 arc minutes over 180 degrees of azimuth resulting in a total of 1800 flats along a 3.14 m arc of a semi-circle. For a field of view of 4 sr with a focal length of 50 cm the mirror flats would be 1 m long along the axial direction. In practice the reflectors would be a two dimensional array of identical mirror modules of moderate size. The reflectors were assumed to be 150 microns thick commercial glass or treated Al foils like those of the ASCA and Suzaku telescopes. They are coated on both faces with Ir or Pt plus a 9nm C overcoat. The mirrors are relatively massive, about 47 kg of glass (51 kg of Al). In the absence of a mechanical design a rule of thumb suggests the structure needed to support the flats would raise the total mass by a factor or 1.5 to 2 for a total telescope mass between 74 and 102 kg.

4.1 Effective area

The effective area and angular resolution in the focusing dimension were estimated by ray tracing. The coded mask, which covers the reflectors, was not included. Its transmission was assumed to be 45% after the fact to account for its 50% open area and to allow loss from support structure. X-ray scattering by a surface with a finite roughness was not included but is expected to be small for this type of glass. Thicker versions of the same material are being used by NuStar and possibly by IXO. The dimensions are chosen such that the system would fit without expansion within the dynamic envelope of “SMEX Fairing B”, which appeared in a previous NASA Small Explorer AO. Considerable volume would be left for spacecraft systems. If the optics were folded the system will fit within the smaller dynamic envelope of the Pegasus spacecraft. The dimensions assumed for the tray tracing appear in Table 1. Without a true engineering design the estimates are tentative. If an analysis reveals that more support structure is required than what was assumed or that the mass is too high for a Pegasus payload, the consequence would be less effective area and/or field of view.

Table 1: Dimensions assumed for the simulation of the 1D lobster-eye telescope

Parameter	**Numerical Value**
Radius of curvature of the detector array, "R", Fig. 1	50 cm, equal to focal length
Circumferential size of the detector array	Up to 1.57 m
Radius of curvature of the reflector array "2R", Fig. 1	100 cm
Circumference of the reflector array, (up to 180 deg)	Up to 3.1 m
Axial length of the array of mirrors	1.0 m*
Axial length of the detector	50 cm*
Azimuth field of view	Up to 180 deg.
Polar angle range with > 0.7 max. area	45 deg. to 135 deg.
Length of the flat reflectors along a radius	6 cm
Angle and physical space between adjacent reflectors	6 arc min and 1.75 mm
Thickness of the reflectors	150 microns
Reflective coating, on both faces of mirror flats	30 nm Ir + 9 nm C
Detector, dimensions of a CMOS or CCD chip	20 mm x 20 mm x 300 microns Si
Number of detector chips	1960
Detector chip packing efficiency	0.8
Detector light shield transmission	Same as Chandra ACIS-S
Coded mask transmission with allowance for structure	0.45

*Either the mirrors or detectors can be larger in the axial direction with the same range of polar angle. Longer mirrors result in a heavier payload; a larger detector array in higher instrument cost and power consumption. In either case both the mirrors and detectors would be a modular array of small identical elements.

The reflectors are distributed along 180 degrees of azimuth. The effective area is independent of the azimuth angle except for very small regions at both ends. In the polar direction the area varies as the cosine of the difference between the polar angle and 90 degrees. To obtain a 4 ster field of view with at least 70% of the maximum area either the detector or the reflector array should be 50 cm high while the other would be 100 cm high. The first option results in a larger, more expensive, higher power consuming detector array but a lower mass mirror. Because the slits of the coded mask are open the full 180 degree azimuth range except for occasional support structure the coded mask does not vignette in the azimuth direction. Vignetting by the coded mask in the polar direction will be small if the mask is thin compared to the ~ 200 micron width of its slits. Tensioned support structure wires or beams can added along the full length of the mask with little loss of area by aligning them with the front of any or all of the 150 micron thick mirrors.

Assuming their dimensions are: 20 mm x 20 mm x 0.3 mm, the number of CMOS or CCD chips, in the focal plane array of detectors is 1,960. By comparison **BAT** of ***Swift*** has 32,768 CZT chips whose dimensions are 4 mm x 4 mm x 2 mm. The total detector area is about 0.7 m^2 in both cases but the lobster detectors with a depth of 0.3 mm of silicon are much lower mass than **BAT**'s 2 mm thick CZT detectors. The level of cosmic ray background in several current missions with X-ray CCD detectors as reported by Hall and Holland, 2010 is very low compared to the level of diffuse cosmic X-ray background expected in this instrument. Therefore, the need for shielding is minimal.

Fig. 3 is a plot of the effective area as a function of energy. It includes factors of 0.45 and 0.80 for the efficiencies of the coded mask and active area of the array of detector chips.

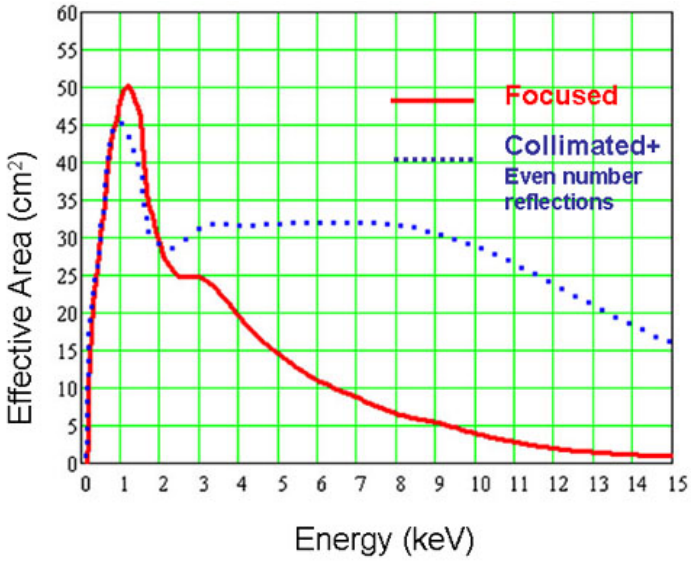

Fig. 3. Effective area at a polar angle of 90 degrees is shown as a function of energy for the focused line image and for X-rays that arrive at detector array without being reflected or are reflected an even number of times. A detector chip packing efficiency of 80% and the Chandra ACIS-S light shield transmission efficiency have been applied. The transmission of the coded mask is assumed to be 45%.

The sensitive absorption depth of the detectors is assumed to 300 microns of Si and the detector has a light shield with the same X-ray transmission properties as the Chandra ACIS-S. The ray tracing results are shown in Tables 2 & 3. The "Focused Area" in Table 2 refers to the rays that appear in the central peaks of the point response functions for the five energies shown in Fig.2. Those rays are reflected an odd number of times but mostly just once.

Table 2 Theoretical Effective Area *

Energy (keV)	**Focused Area (cm^2)**	**Collimated Area & 2 reflections**	**Focused + Collimated & 2 refs.**
0.5	30	31	61
0.75	42	43	85
1	48	45	93
2	29	29	58
5	15	32	47
8	7	32	39
12	2	24	26
15	1	17	18

*Includes transmission of a Chandra ACIS-S type light shield, absorption in a 300 micron thick CMOS or CCD silicon detector chip of an array with 80% packing efficiency. The transmission of the 1D coded mask is 45%.

As shown in Fig. 2 the point response of the lobster-eye telescope is quite unlike that of the Wolter 1 geometry where with the aid of internal baffles the number of rays that reach the focal plane without being reflected are eliminated or minimized. They are unavoidable in the lobster-eye geometry. At low energies the broad distribution of the rays is the result of some X-rays

surviving two, and occasionally four reflections. The fact that both faces of the mirror reflect increases the probability that an X-ray will experience multiple reflections. A ray reflected an even number of times including zero continues along or nearly along its original path. Ray reflected an odd number of times appear in the central peak. Table 3 shows how the power is distributed at 2 keV. There is a broad halo whose surface brightness alternates between zero and a finite value across an angular range of about 3 degrees. On average the surface brightness of the halo is 4% of the central peak.

Table 3 Point Response of lobster-eye telescope at 2 keV

Full angular range of events	3 degrees
Full angular width of central peak	7 arc minutes
Fraction of total power in central peak	0.5
FWHM of central peak	3.5 arc minutes
Fraction of total power within FWHM	0.25

Above 4 keV the number of rays reflected more than once diminishes and the mirrors act as simple reflectors and/or collimators.

According to the ray tracing results the 1D image is a peak above the halo with a full width of 7 arc minutes and a FWHM of 3.5 arc minutes. The effect of the halo is to increase the acceptance of diffuse X-ray background by a factor of 2 up to 3 keV and a larger fraction at higher energies. The precision of the position measurements is the statistical error in determining the centroid of the 3.5 arc minute FWHM central peak. The azimuth angle of sources or bursts with high statistical significance will be measured with sub arc minute precision. Knowing the azimuth angle of the transient from the focused image greatly simplifies the process and improves the accuracy of determining the polar angle by correlating the axial positions of the X-rays with the slits of the 1D coded mask.

5. Sensitivity

5.1 Modeling the sensitivity.

With the exception of a few extended sources notably the Cygnus Loop, the Vela SNR and Puppis A, the image of a discrete source will be significant only over 7 arc minutes of azimuth, because the halo is very low surface brightness. There are 36 sources in the Uhuru catalog whose flux is at least 20% of the crab nebula. In total their 7 arc minute cores will encumber only 4.2 of the 180 degrees of azimuth with a significant increase in the background rate and many of those will be absorbed below 2 keV, leaving the 0.5 to 2 keV band available to the search for transients and other temporal variability. Because the positions of the strong sources are known very accurately they calibrate the system and verify that the process of finding positions is functioning correctly.

All transients will be point sources. We would detect transients by looking for significant increases in the 0.5 to 8 keV band above the background in 7 arc minute bins around the azimuth along the full length of the detector. If a significant increase above background is detected the position of the transient will be obtained by calculating the centroid of the 7 arc minute bins for the azimuth angle. The positions of the counts along the cylinder axis within the 7 arc minute

strip will correlated with the coded mask to obtain the source's polar angle. The source's core image will be distributed over a region of 7 arc minutes x 90 degrees, or 3.2 x 10^{-2} ster. The effective area for estimating the diffuse X-ray background is the sum of the "Focused Area" plus "Collimated Area & 2 reflections" that appear in Table 2. The sum is about a factor of 2.3 larger than the focused area. The 3 degree halo of a source will not add significantly to the detection sensitivity; its surface brightness being only 4% of the 7 arc minute core. However, in the 8 to 16 keV band where the core is very faint the halo still has considerable effective area and providing the event occurs with sufficient intensity can provide useful information on the spectrum and time history of the transient.

Table 4 lists the 7 sigma detection sensitivity in terms of mCrabs for several observing times. The putative source has the same spectrum as the Crab Nebula ($10E^{-2}$ photons/cm^2-sec) including interstellar absorption by a hydrogen column of 3 x 10^{21} H atoms/cm^2 along the line of sight. The spectrum of the diffuse cosmic X-ray background is assumed to $10E^{-2.0}$, E < 1 keV, $10E^{-1.4}$ E > 1keV. The diffuse cosmic X-ray background is more intense at low energies in some regions of the sky but the anisotropies are attenuated considerably because X-rays below 0.5 keV were not included in the simulation, and the Chandra ACIS-S type light shield absorbs significantly below 1 keV.

The system has a field of view of 4 ster with at least 70% of the maximum area plus some more solid angle with less. Not considering possible constraints such as solar avoidance and allowing for 10% loss of time to change pointing positions if all points in the sky were given equal exposure that time would be 24,760 seconds per 24 hours. Table 4 lists the 7 sigma detection sensitivity for various exposure times of a source whose intensity is 10^{-3} of the Crab Nebula.

Table 4 Detection Sensitivity relative to 10^{-3} Crab Nebula

Exposure Time (seconds)	**7 sigma sensitivity, relative to a 1 mCrab source**
30	9.4
100	5.1
10^3	1.2
10^4	0.51
2.47 x 10^4 (One day in LEO)*	0.33

*Equal exposure for all points in sky

5.2 Comparison with other All-Sky Monitors

Comparing a concept with an existing, functioning all-sky monitor has severe limitations. The absence of an engineering design for the lobster-eye telescope where addressing factors such as strength, fit, and the thermal environment could result in reducing the size and degrading the performance of the instrument make comparisons with existing instruments especially dubious. However, the difference between the expected performance of this instrument and the actual performance of the all-sky monitors in orbit is large enough to accommodate a considerable reduction in the performance of the former without changing the conclusion.

Current Instruments: ***RXTE*** **ASM ,MAXI** and **BAT**

The existing all-sky monitors are the ***RXTE*** **ASM,** ***MAXI,*** and the ***Swift*** **BAT. BAT** operates at higher energy than the lobster-eye telescope and should not be compared to a soft X-ray all-sky monitor, which do not detect the same set of variable sources. **BAT** failed to detect the supernova flare caught by chance in a field of the ***Swift*** **XRT,** nor has it detected the X-ray Flashes seen by **BeppoSAX** and **HETE 2.** There also may be "orphan" X-ray afterglows of off-axis GRBs that **BAT** has missed.

Both the ***RXTE*** **ASM** and ***MAXI*** are scanning instruments with a much smaller field of view than the lobster-eye telescope. Their exposure time at a given position is very short. They are not likely to detect a short lived transient such as the 400 second long supernova flare seen in a field of the **XRT.** Also, they would not obtain the complete light curve of the few they could detect. Furthermore, the time when a scanning instrument detects a transient may be several minutes past its start. If they were capable of detecting and determining the position of the event on board there would be a significant delay between its start and the time that the network of ground based robotic and human controlled IR, optical, UV and radio telescopes has enough information to access it.

The sensitivity of both the **ASM** and ***MAXI*** is in the range 10 to 20 milli Crabs per day in "uncrowded fields" (Sugizaki, et al, 2010). The estimated sensitivity of the hybrid lobster-eye telescope described in this paper (Table 4) is a factor of fifty larger. Furthermore, both the **ASM** and ***MAXI*** have a limited lifetime and are unlikely to still be operating in several years. An instrument similar to the ***RXTE*** **ASM** will be aboard ***ASTROSAT***, a project of the Indian Space Research Organization. The launch date is uncertain.

5.3 Comparison with 2D coded mask instruments, including JANUS

The other genre of all-sky telescopes are 2D coded masks, like **BAT** and ***EXIST***, and 2D lobster-eye telescopes. The latter was discussed in Sect. 3.1 and compared to the hybrid 1D telescope + coded mask. The conclusion was that for modest size instruments the smaller area and bandwidth of the 2D telescope, with photon limit and pile-up issues, and its more complex point response rendered it less sensitive and less versatile than the hybrid in detecting and measuring the positions and spectra of fast soft X-ray transients. **BAT** and ***EXIST*** are not in the same category because they operate in a higher energy band where all-sky focusing is not an option.

A 2D coded mask all-sky soft X-ray system would use the same detector system as the hybrid. If the aperture and field of view were the same for both the 2D coded mask would have much more effective area and much higher background. The background would include the discrete X-ray sources as well as the diffuse cosmic X-rays. The 2D coded mask would have to process up to two orders of magnitude more data to find the position of a transient.

The principal advantages of the focusing system are:

(1) The discrete sources, whose flux is considerable in total and often variable, are imaged onto distinct regions of the detector. They do not contribute to the background at other positions and because their positions are known with great accuracy they calibrate the system continuously.

(2) The existence of a burst or transient in the field of the focusing telescope is known virtually instantaneously and its azimuth position is easily determined. The focused line image is seen immediately and the correlation between the axial positions of the events at that azimuth line with the coded mask involves only a very small amount of processing to find an accurate position in the other dimension.

(3) The focusing system is much better equipped to deal with multiple transients or changes in spectra occurring simultaneously such as for example, the time of a variable stellar flare overlapping the time of a GRB or XRF.

(4) The data archive is much more accessible. A light curve for every position in the sky can be compiled very easily.

There is a NASA funded study of a very wide field 2D coded mask instrument for the soft X-ray band, JANUS (Falcone et al, 2009). JANUS may be launched as a Small Explorer mission. The field of view of JANUS and this conceptual instrument is about the same, 4 ster, although the JANUS modules are positioned differently than the cylindrical geometry of the 1D focusing lobster-eye telescope.

Comparing the sensitivity of the hybrid telescope with JANUS is very uncertain because this instrument's configuration is based upon dimensions that have not been validated with a thorough engineering analysis. JANUS's configuration presumably has addressed mass and thermal issues in depth. The nominal sensitivity of the hybrid telescope is 9.4 mCrabs, 7 sigma, 30 seconds exposure, (Table 4), which is much larger than the 240 mCrabs 7 sigma, 30 second sensitivity of JANUS. The effective area is also larger. The bandwidth is about the same if the contribution of the "Collimated Area & 2 reflections" area that appears in Table 3 is included. However, it is difficult to compare the two. The JANUS coded mask is probably much smaller than the hybrid telescope because JANUS accommodates an infrared telescope as part of its payload. The hybrid telescope was not configured to take into account the presence of a another telescope aboard the same Small Explorer type spacecraft. It would have to rely on the network of ground and space based telescopes that respond rapidly to an event to identify the host galaxy and study it at other wavelengths. However, it would be able to detect the burst or transient, determine its position and transient the result to the network very rapidly.

6 Conclusion

The search for bursts and transients and study of soft X-ray variability in general is an important aspect of astronomy in line with similar activity occurring or planned in other wavelength bands. These studies should continue indefinitely. The soft X-ray band, in particular hosts many types of variable sources both galactic and extra-galactic. The range of behaviors include: stellar flares particularly from star formation regions, changes in the intensity and spectrum of neutron star and black hole binaries whose behavior tests the laws of general relativity, activity occurring in the vicinity of supermassive black holes, supernova explosions and the X-ray components of GRBs, XRFs, XRRs and their afterglows. Obtaining a precise position from the X-ray afterglow of a GRB led to finding the most distant object in the universe. The search for ever more distant objects by identifying the host galaxies of bursts will be

strengthened considerably by adding an all-sky X-ray camera that enlarges the scope of the search by encompassing XRFS, and can find precise positions on its own, without the necessity of pointing a separate small field of view telescope. As the host galaxies become more distant the spectrum of a GRB will be increasingly softened by the redshift. At large distances the redshift increases rapidly with distance so the X-ray component of a GRB will be enhanced accordingly.
.

A focusing lobster-eye telescope is a more powerful tool for detecting and finding the position of bursts or transients that may occur at any position in the sky at any time than either a scanning detectors with a limited field of view or a 2D coded mask with a very broad field of view and a high level of background. The hybrid 1D focusing lobster-eye + coded mask is preferable to the current 2D lobster-eye telescopes. It has more effective area and bandwidth for measuring the spectrum and time history of the event. When the transient is faint it is not limited nearly as much by a shortage of photons and when the transient is intense it is not affected by pile-up.

The hybrid telescope would offer peripheral vision to, and find new, interesting targets for the pointed telescopes with very large effective area and very high resolution spectrometers such as IXO to study in-depth.

References

`Angel, J. R. P., 1979, "Lobster eyes as X-ray telescopes", Ap. J. **233**, 364

Bencivenni. G., 2009, "The GEM detector activity at the Frascati Laboratory", Nuclear Physics A, **827**, 614

Bongiorno, S. D., Falcone, A. D., Burrows, D. N., Cook, R., Bai, Y., Farris, M.. 2009, "Measurements of Si hybrid CMOS X-Ray detector characteristics", **SPIE 7435**, 74350E and arXiv:0909.2898.

Chevalier, R. A., Fransson, C. Nymark T.K. 2006, "Radio and X-Ray Emission as Probes of Type IIP supernovae and red supergiant mass loss", ApJ **641,** 1029

Chevalier, R. A.; Fransson, C., 2008, "Shock breakout emission from a Type Ib/c Supernova: XRT 080109/SN 2008D", ApJ **683**, L135

Costa, E.; Frontera, F.; Heise, J.; Feroci, M.; in't Zand, J.; Fiore, F.; Cinti, M. N.; Dal Fiume, D.; Nicastro, L.; Orlandini, M.; Palazzi, E.; Rapisarda, M.; Zavattini, G.; Jager, R.; Parmar, A.; Owens, A.; Molendi, S.; Cusumano, G.; Maccarone, M. C.; Giarrusso, S.; Coletta, A.; Antonelli, L. A.; Giommi, P.; Muller, J. M.; Piro, L.; Butler, R. C., 1997, "Discovery of an X-ray afterglow associated with thegamma-ray burst of 28 February 1997", Nature, **387**, 783

Esquej, P.; Saxton, R. D.; Komossa, S.; Read, A. M.; Freyberg, M. J.; Hasinger, G.; García-Hernández, D. A.; Lu, H.; Zaurín, J. R.; Sánchez-Portal, M.; Zhou, H., 2008, "Evolution of tidal disruption candidates discovered by XMM-Newton, A&A **489**, 543

Falcone, A. Burrows, D., Barthelmy, S., Chang, W., Fredley, J. Kelly, M. Klare, R., Palmer, D., Persyn, S, Reichard, K., Roming, P. Seifert, E., Smith, R.. Wood, P., Zugger, M., 2009, "The JANUS X-Ray Flash Monitor", http://arxiv.org/pdf/0908.3005

Fiore, F.; D'Elia, V.; Lazzati, D.; Perna, R., Sbordone, L., Stratta, G., Meurs, E. J. A.; Ward, P., Antonelli, L. A., Chincarini, G.; Covino, S.; Di Paola, A.; Fontana, A.; Ghisellini, G.; Israel, G.; Frontera, F.; Marconi, G.; Stella, L.; Vietri, M.; Zerbi, F., 2005
"A Flash in the Dark: UVES Very Large Telescope High-Resolution Spectroscopy of Gamma-Ray Burst Afterglows", ApJ **624,** 853

Fraser, G. W. et al (29 other authors), 2002, "Lobster-ISS: An Imaging X-ray all-sky monitor for the International Space Station", **SPIE 4497**, 115

Gehrels, N. on behalf of the Swift team, 2004, "The Swift γ-ray burst mission", New Astronomy Reviews, **48**, 431

Gorenstein, P. and Mauche, C. W., 1984, "All Sky High Resolution Cameras for Hard and Soft X-rays" in AIP Conference Proceedings No. 115, High Energy Transients in Astrophysics, S. Woosley Ed., 694

Gorenstein, P., Whitbeck, E., Austin, G.A, Kenter, A., Pina, L., Inneman, A., and Hudec, R., 1996, "A lobster eye X-ray telescope prototype", **SPIE 2805**, 74

Grindlay, J. 2005, "EXIST: All-sky hard X-ray imaging and spectral–temporal survey for black holes", New Astronomy Reviews **79**, 436

Grubsky, Victor; Gertsenshteyn, Michael; Shoemaker, Keith; Jannson, Tomasz, 2007, "Adaptive lobster-eye hard x-ray telescope with high-angular resolution and wide field of view", **SPIE.6688**, 66880P

Hall, D. J. and Holland, A. 2010, "Space radiation environment effects onX-ray CCD background", Nuclear Instruments and Methods in Physics Research A, **612**, 320

Halpern, J. P.; Gezari, S.; Komossa, S., 2004, "Follow-Up Chandra Observations of Three Candidate Tidal Disruption Events", ApJ **604**, 572

Heise, J.; in't Zand, J., Kippen, R. M., Woods, P. M., 2001, "X-Ray Flashes and X-Ray Rich Gamma Ray Bursts", presented at Gamma-Ray Bursts in the Afterglow Era: Proceedings of the International Workshop Held in Rome, Italy, 17-20 October 2000, ESO ASTROPHYSICS SYMPOSIA. ISBN 3-540-42771-6. Edited by E. Costa, F. Frontera, and J. Hjorth. Springer-Verlag, 16

Hudec, Rene; Inneman, Adolf V., Pina, Ladislav; Hudcova, V., Sveda, L., Ticha, Hana, 2003, "Lobster-eye x-ray telescopes: recent progress", **SPIE 4851**, 578

Janesick, J., Pinter, J., Potter, R., Elliott, T. Andrews, J, Tower, J., Cheng, J., Bishop. J. 2009. "Fundamental performance differences between CMOS and CCD imagers: Part III", **SPIE 7439**, 7439A-6

Land, M.F.1978, "Animal eyes with mirror optics", Scientific American **239 (6),** 88

Matsuoka, M.; Kawasaki, K.; Ueno, S.; Tomida, H.; Kohama, M.; Ishikawa, M.; Katayama, H.; Suzuki, M.; Miyakawa, T.; Mihara, T.; Isobe, N.; Tsunemi, H.; Miyata, E.; Negoro, H.; Nakajima, M.; Kawai, N.; Kataoka, J.; Yoshida, A.; Yamaoka, K.; Morii, M., 2007, "An overview of MAXI onboard JEM-EF of the International Space Station", **SPIE 6686**, 668611

Mitsuishi, I.,, Ezoe, Y, Koshiishi, M., Mita, M., Maeda, Y., Yamasaki, N. Mitsuda, K., Shirata, T. Hayashi, T., Takano, T., Maeda, R., 2010, "Evaluation of the soft x-ray reflectivity of micropore optics using anisotropic wet etching of silicon wafers", Applied Optics 49, 1007

Mutz, Jean-Luc; Bonnet, Olivier; Fairbend, Ray; Schyns, Emile; Seguy, Julien, 2007, "Micro-pore optics: from planetary x-rays to industrial market", **SPIE 6479**, 6479F

Remillard, R., Levine, A., and McClintock, J., 2009 "Scientific Productivity with X-ray All-Sky Monitors", arXive:0903.3195v1 (Astro-ph.HE)

Risaliti, G.; Miniutti, G.; Elvis, M.; Fabbiano, G.; Salvati, M.; Baldi, A.; Braito, V.; Bianchi, S.; Matt, G.; Reeves, J.; Soria, R.; Zezas, A., 2009, "Variable Partial Covering and A Relativistic Iron Line in NGC 1365", ApJ **696**, 160

Rossi, E., Perna, R , Daigne, F., 2008, "Orphan' afterglows in the Universal structured jet model for γ -ray bursts", Mon. Not. R. Astron. Soc. 390, 675

Sakamoto, T, et al (35+ other authors), 2005, "Global Characteristics of X-Ray Flashes and X-Ray-Rich Gamma-Ray Bursts Observed by HETE-2", ApJ **629**, 311

Salvaterra, R. and 24 co-authors, 2009, "GRB090423 at a redshift of z~8.1". Nature **461**, 1258

Schmidt, W. K. H., 1975, "A proposed X-ray focusing device with wide field of view for use in X-ray astronomy", Nuclear Instruments and Methods **127**, 285

Soderberg, A. and 40 co-authors, 2008, "An extremely luminous X-ray outburst at the birth of a supernova", Nature **453**, 469

Soderberg, A. and many co-authors, 2009, "The Dynamic X-ray Sky of the Local Universe", A White Paper Submitted to the Astronomy Decadal Survey Committee
http://sites.nationalacademies.org/BPA/BPA_050603

Sugizaki, Mutsumi; MAXI collaboration, 2010, "Monitor of X-ray transients with MAXI GSC on board ISS", 2010HEAD...11.1302S

Tanvir, N. R. and 62 co-authors, 2009, "A big gamma-ray burst at a redshift of z approximately 8.2", Nature **461**, 1254

Wang, J, Risaliti, G., Fabbiano, G., Elvis, M. ,Zezas, A, and Karovska, M. 2010, "Revisit short term X-ray spectral variability of NGC 4151 with Chandra", ApJ (in press)

Woods, E., Loeb, 1999, "Constraints on off-axis x-ray emission from beamed gamma-ray bursts", ApJ 523, 187

Woosley, S. E. and Bloom, J. S., 2006, "The Supernova Gamma-Ray Burst Connection", Annual Rev. Astron. Astrophys. **2006**, 44